

PHP-Based Coverage Analysis in Millimeter Wave Heterogeneous Cellular Network

Mehdi Sattari and Aliazam Abbasfar, *Senior Member, IEEE*

Abstract

With severe spectrum shortage and high capacity requirement in future cellular networks, millimeter wave (mmWave) frequencies is a candidate for next-generation wireless networks. Due to the sensitivity of mmWave signals to blockage and using directional beamforming in both transmitter and receiver, novel models are needed to analyze cellular networks operating in mmWave frequencies. Base station (BS) locations in heterogeneous cellular networks (HCNs) is often modeled by a Poisson point process (PPP). While it is a proper model due to the randomness of BS locations, it can not accurately model the network when we have multi-tiered BSs, e.g. macro cells and small cells. The effect of spatial separation between tiers leads us to model BS locations as a Poisson hole process (PHP). Using tools from stochastic geometry, this paper proposes a framework to evaluate the coverage performance in a two-tier mmWave HCN. Since the exact formulation of coverage probability based on PHP modeling of SBSs is not known, different approaches are proposed and fairly accurate expressions for coverage probability are derived and validated by simulation results. It turns out that the analysis based on the proposed model is more accurate for a two-tier HCN than independent PPP-based analysis.

Index Terms

Millimeter wave cellular network, heterogeneous cellular network, stochastic geometry, Poisson Hole Process, coverage probability.

I. INTRODUCTION

The explosive growth of mobile data traffic in recent years and spectrum shortage in microwave bands have motivated the use of new frequency bands for cellular communication. To that end, millimeter wave (mmWave) communications have been proposed to be an important part of the 5G mobile network to provide high data-rate communication services [1], [2], [3]. Despite massive amounts of bandwidth available in mmWave bands, they have been traditionally considered only for long distance point-to-point communication such as satellite or short range

indoor communications. But recent channel measurements in [2] have been revealed that they can be used for commercial cellular systems.

Due to fundamental propagation differences between mmWave and microwave frequencies, it is not possible to use prior models for cellular networks operating in microwave bands [4]. Because of small wavelength and small antenna aperture, path loss in mmWave frequencies is larger than microwave frequencies. On the other hand, it is possible to use antenna arrays in mmWave transceivers to provide high array gain, by beamforming, and compensate for large path loss. Another distinguishing feature of mmWave frequencies is sensitivity to blockage. This effect needs to be incorporated in models for analyzing mmWave networks. Channel measurements have revealed that there are some differences in the line of sight (LOS) and non-line of sight (NLOS) links in these bands [2]. For this reason, different path loss exponents in LOS and NLOS links are used for system models.

A. Related Work

Significant progress has been recently made to analyze the cellular networks performance using tools from stochastic geometry. Characterization of signal-to-interference-and-noise ratio (SINR) distribution in cellular networks was pioneered by [5], which provides a mathematical framework for downlink SINR distribution. Stochastic geometry-based analysis for mmWave cellular networks was first done in [6]. Incorporating blockage effect and directional beamforming in network analysis of mmWave cellular system was applied in [4] and a comprehensive mathematical model was provided. The results in [4] revealed that mmWave cellular networks can outperform conventional cellular networks in terms of SINR coverage and average rate. Furthermore, a simplified blockage model named LOS ball model was introduced in [4]. It was later extended by [7], in which a tractable model for data-rate was developed in self-backhauled mmWave cellular networks.

Heterogeneous cellular network (HCN) is modeled as a multi-tiered cellular network where the base stations (BSs) of each tier are randomly distributed and have a particular transmit power and spatial density. A general model for HCNs assumes K independent tiers of Poisson point process (PPP) distributed BSs, which is the most simplified model in the literature. Some tractable models for SINR distribution in a general K -tier downlink HCN have been developed in [8], [9], [10]. Employing similar approaches from stochastic geometry used in microwave frequency and

incorporating the distinguishing features of mmWave frequency, in [11] heterogeneous downlink mmWave cellular networks was studied.

Although most of the stochastic geometry works on HCNs focus on PPP-based deployment of BSs, it is unrealistic to assume that the locations of the BSs corresponding to different tiers are completely uncorrelated. Therefore, the effect of spatial separation between tiers are usually overlooked and modeling HCNs accounting for the spatial dependence should be devised. In [12] two different cases, inter-tier dependence and intra-tier dependence, are considered for a two-tier HCN. Each of the two cases introduces one form of dependence between the locations of macro and small cells. In such a setup, the small cell locations are modeled by a Poisson hole process (PHP) and Matern cluster process (MCP). A comprehensive analysis for PHP is developed in [13], where the Laplace transform of the interference is derived by considering the local neighborhood around a typical node of a PHP. In [14], lower bounds on the cumulative distribution function (CDF) of the contact distance in a PHP for two different cases are derived and compared with previous approximations.

PHP has also various applications in modeling wireless networks such as device-to-device (D2D) networks and cognitive radio networks. In D2D networks, D2D transmissions have an exclusion region around each transmitter and the remaining active D2D transmitters are modeled by a PHP [15]. In cognitive radio networks, a secondary user equipment (UE) may transmit only when it is outside the primary exclusion regions [16] to avoid harmful interference to primary UEs. In this case, the spatial distribution of active secondary UEs forms a PHP.

To the best of authors' knowledge, there is no comprehensive analysis for mmWave HCN with spatial separation between macro cell BSs (MBSs) and small cell BSs (SBSs). Using LOS ball model introduced in [4] for blockage, and approximating interference with a similar approach developed in [12], [17] derived the SINR distribution for a non-uniform mmWave HCN. In this paper, incorporating distinguishing features of mmWave communications, i.e. sensitivity to blockage and directional beamforming in mmWave transmitters and receivers, an appropriate system model is proposed and different analytical expressions for SINR coverage probability are derived.

B. Contribution

In this paper a two-tier HCN is considered whose tiers are spatially correlated, i.e. SBSs are not deployed inside the coverage area of MBSs. We consider circular sector holes centered at

MBS locations and in a random direction, which can be a reasonable assumption because of differences in mmWave propagation. For instance, an operator may deploy an SBS close to an MBS due to possible blockage or negligible side lobe array gain. It should be noted that our analysis can be easily extended to circular holes, which is the default configuration of holes in the definition of PHP [18].

The traditional approach to analyze the coverage for such networks is to ignore the holes and model the BSs as homogeneous independent PPP. This is considered as the baseline approach in our paper, and we compare our other proposed approaches with it. The exact analysis of SINR coverage probability is not possible due to the complexity of PHP-based location of SBSs and correlation between two tiers. Hence, the main focus of this paper is to derive some tractable analytical expression for the performance of such networks. We take some different approaches to tackle this problem that we describe briefly in the following:

- In the first approach, we ignore the effect of holes and approximate PHP by the baseline PPP of SBSs and analytical expressions for SINR distribution are derived in a mmWave HCN with a general LOS probability function. This approach actually is the same as when HCN is modeled by homogeneous independent PPP and provide a lower bound for coverage probability. Also as a corollary, we approximate PHP by PPP with the same density. This approach is common in the papers that deal with PHP. By calculating the density of PHP and using properties of PPP an approximation for coverage probability is provided.
- In the second approach, we consider the effect of holes when the typical UE is associated with an MBS and by incorporating the *serving hole*, and an analytical expression for SINR coverage probability is derived.
- In the third approach, we incorporate the nearest non-serving LOS and NLOS holes, which gives a more complex analysis than prior approaches but still tractable.
- In the fourth approach, the effect of all non-serving holes are incorporated, but we ignore possible overlaps between them. Moreover, to reduce the impact of the approximation used in deriving the analytical expression, we incorporate all holes that are outside of a given radius from the typical UE.

C. Organization

The rest of the paper is organized as follows. In section II, considering features of mmWave communications, our system model is introduced. In section III, SINR coverage probability of the

TABLE I: Notation and Description

Symbol	Description
ϕ_1, λ_1	PPP distribution of MBSs, density of ϕ_1
ϕ_2, λ_2	baseline PPP distribution of SBSs, density of ϕ_2
ψ, λ_{PHP}	PHP distribution of SBSs, density of ψ
ϕ_u, λ_u	PPP distribution of UEs, density of ϕ_u
$BS_{k,0}$	serving BS
P_k	transmission power of BS in k^{th} tier
G_k	directivity gain of BS in k^{th} tier
θ_k	beamwidth of BS in k^{th} tier
θ_{UE}	beamwidth of UE
$ h_{j,i} ^2$	channel gain between the typical UE and the i^{th} BS in the j^{th} tier
α^s	$s \in \{LOS, NLOS\}$ path loss exponent
v^s	$s \in \{LOS, NLOS\}$ Nakagami parameter
$P^s(r)$	$s \in \{LOS, NLOS\}$ probability
P_C	SINR coverage probability
$S(x, D, \theta_c)$	circular sector with radius D and central angle θ_c centered at x

network based on different approaches is derived. In Section IV, numerical results are presented to compare and validate different analytical expressions proposed in section III and the impact of the system parameters on the performance evaluation are identified. Finally, conclusions and suggestion remarks for future works are provided in section V.

II. SYSTEM MODEL

In this section, we describe our system model for evaluating coverage performance of a two-tier mmWave HCN. A brief overview of notations used in the system model and their descriptions have been summarized in Table I.

A. BS and UE Locations

The BSs in all tiers are operating in mmWave band with transmit power P_k , $k = 1, 2$. The location of MBSs are distributed as a homogeneous PPP of density λ_1 and the location of SBSs are treated as a PHP. Each MBS has an exclusion region that is a circular sector centered at the location of the MBS, with radius D , and central angle θ_c . A typical realization of MBSs and SBSs are shown in Fig. 1. Such employing SBS locations improve the network capacity and fills coverage holes better. We elaborate more on the properties of a PHP below.

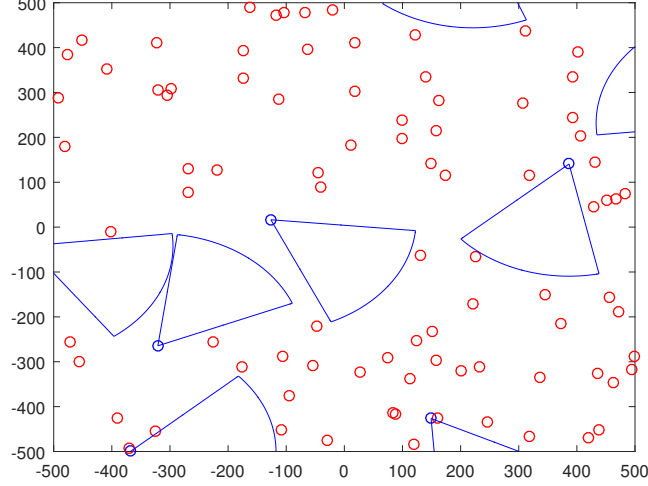


Fig. 1: Two-tier HCN with spatial separation between tiers. The blue circles are the MBSs and circular sectors are exclusion regions with radius D and central angle θ_c . The red circles are SBSs deployed outside the exclusion regions.

Definition 1 (Poisson Hole Process). A PHP is constructed by two independent PPPs: $\phi_1 \equiv \{x\} \subset \mathbb{R}^2$ of density λ_1 and ϕ_2 of density λ_2 . The first process represents the hole centers, i.e. locations of MBSs, and the second process represents the baseline process for SBSs before excluding those who fall in the holes. For each $x \in \phi_1$ we remove all the points in $\phi_2 \cap S(x, D, \theta_c)$, where $S(x, D, \theta_c)$ is a circular sector with radius D and central angle θ_c centered at the location of the points in ϕ_1 . Then, the remaining points in ϕ_2 form the PHP ψ , which can be mathematically defined as

$$\psi = \{y \in \phi_2 : y \notin \bigcup_{x \in \phi_1} S(x, D, \theta_c)\} \quad (1)$$

The UEs are spatially distributed according to another homogeneous PPP and independent of BSs process, which is denoted by ϕ_u of density λ_u . The typical UE is assumed to be at the origin. Due to Slivnyak's theorem, this assumption does not change the statistical properties of the desired distribution [18].

B. Blocking

Recent experimental results have revealed a high sensitivity of received signals to blockage at mmWave frequencies. Therefore, the path loss in LOS and NLOS links are quite different. So,

theoretical works in [4], [7] have used different path loss exponents to model LOS and NLOS channels. Due to irregular building deployments, the links in the network can be either LOS or NLOS randomly, which can be modeled as a stochastic blockage proposed in [19] based on random shape theory. According to this model, a LOS probability is defined as a deterministic non-increasing function of distance denoted as $P^{LOS}(r)$, where r is the distance between BSs and the typical UE. For mathematical simplicity, different approximations have been used for LOS probability $P^{LOS}(r)$. For example, in [4] a LOS ball model is introduced, where LOS probability is equal to one inside of a ball and it is zero outside of the ball. In other words, the links inside the ball are assumed to be LOS and the rest are all NLOS. There are also more generalized models in some papers such as [20], where piece-wise LOS probability function and multi-ball models are used. In this paper, we have used the general LOS probability function $P^{LOS}(r)$ for our analysis.

For this scenario, mmWave BSs are divided into two sub-processes in each tier: the LOS BSs and the NLOS BSs. Therefore, the LOS and NLOS BSs form two independent non-homogeneous PPPs ϕ_k^{LOS} and ϕ_k^{NLOS} in each tier, of density $\lambda_k P^{LOS}(r)$ and $\lambda_k(1 - P^{LOS}(r))$ respectively. Similarly, we have two independent ψ^{LOS} and ψ^{NLOS} for SBS locations as well.

C. Beamforming

Antenna arrays at MBSs, SBSs, and UEs are assumed to perform directional beamforming. A desirable advantage of such deployment is interference isolation, which reduces the impact of the intercell interference. The typical UE and its serving BS are assumed to have perfect channel state information (CSI) and can adjust the angles of the departure and arrival to achieve the maximum array gains. The beam direction of the interfering links is independently and uniformly distributed in the range $[0, 2\pi)$. We approximate the actual array pattern by the sectorized antenna model introduced in [4]. Based on this model, the directivity gain G_k in each tier is a discrete random variable with the value $A_{k,g}$ and probability $P_{k,g}$ ($g = 1, 2, 3, 4$), where $A_{k,g}$ and $P_{k,g}$ are constants defined in Table II and $c_k = \frac{\theta_k}{2\pi}$, $c_{UE} = \frac{\theta_{UE}}{2\pi}$. Sectorized antenna model is the most traditional and tractable approximation for actual array beam pattern that has been adopted in [4], [7], [21], [11]. Due to practical issues and imperfect CSI, alignment of narrow beamwidth at BSs and UEs may be difficult. So, in [21] beamforming alignment error has been considered for a more accurate analysis of mmWave cellular systems. However, we use this model without alignment errors consideration in this paper.

TABLE II: Probability mass function of directivity

g	1	2	3	4
$A_{k,g}$	$M_k M_{UE}$	$M_k m_{UE}$	$m_k M_{UE}$	$m_k m_{UE}$
$P_{k,g}$	$c_k c_{UE}$	$c_k (1 - c_{UE})$	$(1 - c_k) c_{UE}$	$(1 - c_k)(1 - c_{UE})$

D. Path Loss and Fading

As discussed in blocking model, different path loss exponents are applied to LOS and NLOS links. Therefore, we define the path loss for each tier as below:

$$L(r) = \begin{cases} r^{-\alpha^{LOS}} & w.p. \quad P^{LOS}(r) \\ r^{-\alpha^{NLOS}} & w.p. \quad P^{NLOS}(r) \end{cases} \quad (2)$$

where α^{LOS} and α^{NLOS} are LOS and NLOS path loss exponents and $P^{NLOS}(r) = 1 - P^{LOS}(r)$. There are other path loss models such as [22], in which multi-slope path loss models are proposed. However, we use the standard path loss model given in (2) in this paper.

Due to minor small-scale fading in mmWave cellular systems, we assume independent Nakagami fading for each link, which is more general than Rayleigh fading used to model fading in conventional cellular networks. Also, different parameters of Nakagami fading ν^{LOS} and ν^{NLOS} are assumed for LOS and NLOS links and they are assumed to be positive integers for simplicity. Based on Nakagami fading assumption, the channel gain between the UE and BSs are normalized Gamma random variables. Shadowing is ignored in our system model but can be incorporated similar to [7].

E. Cell Association

We consider the following cell association rule: The typical UE is associated with the strongest BS in terms of long-term averaged received power at the typical UE. We assume that the typical UE is allowed to access either an MBS or an SBS. Therefore, the typical UE is associated with a $s \in \{LOS, NLOS\}$ BS in k^{th} tier if and only if

$$P_k G_k r_k^{-\alpha^s} > P_j G_j r_j^{-\alpha^{s'}} \quad (3)$$

where P_k , G_k , $r_k^{-\alpha^s}$, $r_j^{-\alpha^{s'}}$ denote the transmission power, directivity gain in the serving link and path loss in k^{th} and j^{th} tier for $(k, j = 1, 2)$ and state $s, s' \in \{LOS, NLOS\}$. It is worth noting that there are other cell association schemes used in cellular networks, such as instantaneous

power based cell association or average biased-power cell association [10], that can be used similarly in our developed network analysis framework.

III. SINR COVERAGE PROBABILITY

In this section, we evaluate the coverage probability of a two-tier HCN under the system model given in Section II and derive expressions for SINR distribution in a mmWave network with general LOS probability function $P^{LOS}(r)$.

In a multi-tier scenario, the serving BS may not always be the nearest BS for a given UE. However, it is obvious that serving BS is one of the closest BS from a given tier. We first derive the probability density function (PDF) of the distance separating the typical UE and the closest LOS/NLOS BS in each tier, which will be used in the upcoming analysis.

Lemma 1 (Distance to the nearest $s \in \{LOS, NLOS\}$ BS in k^{th} tier). *Given that the typical UE observes at least one $s \in \{LOS, NLOS\}$ BS in k^{th} tier, the conditional PDF of distance to the nearest $s \in \{LOS, NLOS\}$ BS in k^{th} tier is*

$$f_k^s(r) = A_k'^s([0, r)) \exp(-A_k^s([0, r))) / B_k^s \quad (4)$$

where

$$A_k^s([0, r)) = 2\pi\lambda_k \int_0^r x P^s(x) dx, \quad A_k'^s([0, r)) = 2\pi\lambda_k r P^s(r) \quad (5)$$

and $B_k^s = 1 - \exp(-A_k^s([0, \infty)))$ is the probability that the typical UE observes at least one $s \in \{LOS, NLOS\}$ BS in k^{th} tier.

Proof. The proof is similar to [4] and can be derived using the null probability of a 2-D Poisson process. ■

Next, we calculate the association probability given in lemma 2.

Lemma 2 (Association probability). *The probability that the typical UE is associated with a $s \in \{LOS, NLOS\}$ BS in k^{th} tier for $k = 1, 2$ is*

$$A_k^s = \int_0^\infty A_k'^s([0, x)) \exp\left(-\sum_{j=1}^2 \sum_{s' \in \{LOS, NLOS\}} A_j^{s'}([0, R_j^{s'}(x)))\right) dx \quad (6)$$

where

$$R_j^{s'}(x) = \left(\frac{P_j}{P_k} \times \frac{M_j}{M_k}\right)^{1/\alpha^{s'}} \times x^{\alpha^s/\alpha^{s'}} \quad (7)$$

is the exclusion radius of the $s' \in \{LOS, NLOS\}$ interferer BSs in j^{th} tier, when typical UE is associated with a $s \in \{LOS, NLOS\}$ BS in k^{th} tier.

Proof. See Appendix A. ■

Since the location of SBSs is a PHP, thoroughly incorporating the hole effects in the PDF and the association probability makes the analytical expression of coverage probability very difficult. In this paper, we focus on deriving a simpler and more tractable analysis. Therefore, we ignore the holes in deriving the PDF and the association probability and only consider them in the interference characterization. Numerical results in [14] for distance distribution in PHP have revealed that such an approximation has negligible error compared to true PHP-based PDF.

Now we are prepared to develop a theoretical framework to analyze the downlink coverage probability for the typical UE. Based on the system model proposed in section II, SINR received by the typical UE when the typical UE is associated with a $s \in \{LOS, NLOS\}$ BS in k^{th} tier can be expressed as

$$SINR_k^s = \frac{P_k |h_{k,0}|^2 G_{k,0} r_k^{-\alpha_s}}{\sigma^2 + I} \quad (8)$$

where σ^2 is thermal noise power and $|h_{j,i}|^2$ is the channel gain between the typical UE and i^{th} BS in j^{th} tier, and I is the cumulative interference that the typical UE experience from all the other BSs, which is

$$I = \sum_{s' \in \{LOS, NLOS\}} \sum_{i \in \{\phi_1^{s'}\} \setminus BS_{k,0}} P_1 |h_{1,i}|^2 G_{1,i} r_{1,i}^{-\alpha_{s'}} + \sum_{s' \in \{LOS, NLOS\}} \sum_{i \in \{\psi^{s'}\} \setminus BS_{k,0}} P_2 |h_{2,i}|^2 G_{2,i} r_{2,i}^{-\alpha_{s'}} \quad (9)$$

and has two components: Interference from the BSs operating in the same cell with the $BS_{k,0}$ (intracell interference), and from the BSs in other cells (intercell interference). Having assumed the perfect beam alignment of the serving BS and the typical UE, we have $G_{k,0} = M_k M_{UE}$.

As discussed in section II, spatial distribution of the MBSs can be decomposed into two independent non-homogeneous process: the LOS process ϕ_1^{LOS} and NLOS process ϕ_1^{NLOS} . Similarly, we have ψ^{LOS} and ψ^{NLOS} for PHP distribution of SBSs. Therefore, the SINR coverage probability (P_C) of the network can be computed using the total probability law as follows

$$P_C = Pr(SINR > \tau_k) = \sum_{k=1}^2 \sum_{s \in \{LOS, NLOS\}} A_k^s P_{C_k}^s(\tau_k) \quad (10)$$

where $P_{C_k}^s(\tau_k)$ and A_k^s is the conditional coverage and association probability given that the typical UE is associated with a $s \in \{LOS, NLOS\}$ BS in k^{th} tier. In the following sections, we calculate coverage probability for a two-tier mmWave HCN using a few different approaches.

A. Approximating PHP by baseline PPP

In this approach, PHP distribution of SBSs is approximated by baseline PPP ϕ_2 . This approach is the same as modeling SBSs as PPP, which ignores the correlation between the location of BSs of different tiers. This approach underestimates the coverage probability and hence leads to a lower bound. Next theorem provides coverage probability based on this approximation.

Theorem 1. *The PPP-based coverage probability for a two tier mmWave HCN is*

$$P_C \approx \sum_{k=1}^2 \sum_{s \in \{LOS, NLOS\}} \sum_{n=1}^{v^s} (-1)^{n+1} \binom{v^s}{n} \int_0^\infty \exp(-\mu_{k,n}^s \sigma^2) \exp\left(-\sum_{j=1}^2 \sum_{s' \in \{LOS, NLOS\}} \{W_j^{s'}(x) + \Lambda_j^{s'}([0, R_j^{s'}(x)])\} \times \Lambda_k^{s'}([0, x])\right) dx \quad (11)$$

where

$$W_j^{s'}(x) = \sum_{g=1}^4 P_{j,g} \int_{R_j^{s'}(x)}^\infty F(v^{s'}, \frac{\mu_{k,n}^s P_j A_{j,g} r^{-\alpha^{s'}}}{v^{s'}}) \Lambda_j^{s'}([0, r]) dr \quad (12)$$

and $F(v, x) = 1 - (\frac{1}{1+x})^v$, $\mu_{k,n}^s = \frac{n\tau_k\eta^s}{P_k G_{k,0} x^{-\alpha^s}}$, $\eta^s = \nu^s (\nu^s!)^{-1/\nu^s}$.

Proof. See Appendix B. ■

As a consequence, using independent thinning of a PPP, we approximate PHP distribution of SBSs by a PPP with the same density, i.e. density of ψ . Therefore, we need to derive the density of ψ denoted by λ_{PHP} . Similar to [13], it is easy to see $\lambda_{PHP} = \lambda_2 \exp(-\lambda_1 \theta_c D^2/2)$. Based on this density, we define $\Lambda_{k,PHP}^s$ as follows

$$\Lambda_{1,PHP}^s([0, r]) = \Lambda_1^s([0, r]), \quad \Lambda_{2,PHP}^s([0, r]) = 2\pi\lambda_{PHP} \int_0^r x P^s(x) dx \quad (13)$$

and

$$\Lambda_{1,PHP}^{s'}([0, r]) = \Lambda_1^{s'}([0, r]), \quad \Lambda_{2,PHP}^{s'}([0, r]) = 2\pi\lambda_{PHP} r P^s(r) \quad (14)$$

Now, to derive the coverage probability in this case, it is enough to replace $\Lambda_k^s([0, r])$ with $\Lambda_{k,PHP}^s([0, r])$ in the equation (11). The result is stated below for completeness.

Corollary 1. *The coverage probability when PHP is approximated by a PPP with same density is*

$$P_C \approx \sum_{k=1}^2 \sum_{s \in \{LOS, NLOS\}} \sum_{n=1}^{v^s} (-1)^{n+1} \binom{v^s}{n} \int_0^\infty \exp(-\mu_{k,n}^s \sigma^2) \exp\left(-\sum_{j=1}^2 \sum_{s' \in \{LOS, NLOS\}} \{W_j^{s'}(x) + \Lambda_{j,PHP}^{s'}([0, R_j^{s'}(x)])\} \times \Lambda_k^{s'}([0, x])\right) dx \quad (15)$$

B. Incorporating serving hole

To provide more accurate coverage probability, we incorporate only the effect of the serving hole in our analysis. The term serving hole used in this paper represents the hole that is associated with the serving MBS. Since serving MBS is the closest LOS/NLOS MBS to the typical UE, serving hole is the nearest LOS/NLOS hole to the typical UE. However, in the case when the typical UE is associated with a LOS MBS, it is possible that some non-serving NLOS MBSs exist who are closer to the typical UE, hence, their holes are closer than serving hole as well.

Theorem 2. *The coverage probability by incorporating serving hole can be evaluated as*

$$P_C \approx \sum_{k=1}^2 \sum_{s \in \{LOS, NLOS\}} \sum_{n=1}^{v^s} (-1)^{n+1} \binom{v^s}{n} \int_0^\infty \exp(-\mu_{k,n}^s \sigma^2) \exp\left(-\sum_{j=1}^2 \sum_{s' \in \{LOS, NLOS\}} \{W_j^{s'}(x) + \Lambda_j^{s'}([0, R_j^{s'}(x)])\} \times \exp\left(\sum_{s' \in \{LOS, NLOS\}} Q^{s'}(x) \mathbb{1}(k=1)\right) \Lambda_k^{s'}([0, x])\right) dx \quad (16)$$

where

$$Q^{s'}(x) = \frac{\theta_c}{2\pi} \lambda_2 \sum_{g=1}^4 P_{2,g} \int_0^{2\pi} \int_0^D F(v^{s'}, \frac{\mu_{k,n}^s P_2 A_{2,g} (u^2 + x^2 - 2ux \cos(\varphi))^{-\alpha^{s'}/2}}{v^{s'}}) P^{s'}((u^2 + x^2 - 2ux \cos(\varphi))^{1/2}) u du d\varphi \quad (17)$$

and $\mathbb{1}(\cdot)$ is the indicator function.

Proof. See Appendix C. ■

C. Incorporating nearest non-serving LOS and NLOS holes

By ignoring all the holes except the nearest non-serving LOS and NLOS ones, we evaluate the coverage performance of the network. In other words, in this approach, we consider the nearest holes that are associated with the interferer MBSs, i.e. the MBSs who are not serving the typical

UE, and therefore, the effect of the serving hole has not taken into account in this approach. Note that the term LOS/NLOS hole used in this paper represents the hole that is associated with the LOS/NLOS MBS.

Theorem 3. *The coverage probability by incorporating the nearest non-serving LOS and NLOS holes can be expressed as*

$$P_C \approx \sum_{k=1}^2 \sum_{s \in \{LOS, NLOS\}} \sum_{n=1}^{v^s} (-1)^{n+1} \binom{v^s}{n} \int_0^\infty \exp(-\mu_{k,n}^s \sigma^2) \exp\left(-\sum_{j=1}^2 \sum_{s' \in \{LOS, NLOS\}} \{W_j^{s'}(x) + \Lambda_j^{s'}([0, R_j^{s'}(x)])\} \times Z(x) \Lambda_k^{s'}([0, x])\right) dx \quad (18)$$

where

$$Z(x) = \prod_{s'' \in \{LOS, NLOS\}} \int_{R_1^{s''}(x)}^\infty \exp\left(\sum_{s' \in \{LOS, NLOS\}} Q^{s'}(y)\right) \frac{\Lambda_1^{s''}([0, y]) \exp(-\Lambda_1^{s''}([0, y]) + \Lambda_1^{s''}([0, R_1^{s''}(x)]))}{1 - \exp(-\Lambda_1([R_1^{s''}(x), \infty)))} dy \quad (19)$$

and $R_1^{s''}(x) = (\frac{P_1}{P_k} \times \frac{M_1}{M_k})^{1/\alpha^{s''}} \times x^{\alpha^s/\alpha^{s''}}$ is the exclusion radius of the $s'' \in \{LOS, NLOS\}$ interferer MBSs, when typical UE is associated with a $s \in \{LOS, NLOS\}$ BS in k^{th} tier.

Proof. See Appendix D. ■

D. Incorporating all non-serving holes

In this approach, we provide an analytical expression for the coverage probability by incorporating all non-serving holes. However, here the overlaps between them are ignored. Due to possible overlaps among holes, there are some points that will be removed multiple times. Note that similar to Theorem 3, the effect of the serving hole has not been considered in this approach.

Theorem 4. *The coverage probability by incorporating all non-serving holes is*

$$P_C \approx \sum_{k=1}^2 \sum_{s \in \{LOS, NLOS\}} \sum_{n=1}^{v^s} (-1)^{n+1} \binom{v^s}{n} \int_0^\infty \exp(-\mu_{k,n}^s \sigma^2) \exp\left(-\sum_{j=1}^2 \sum_{s' \in \{LOS, NLOS\}} \{W_j^{s'}(x) + \Lambda_j^{s'}([0, R_j^{s'}(x)])\} \times T(x) \Lambda_k^{s'}([0, x])\right) dx \quad (20)$$

where

$$T(x) = \exp\left(-\sum_{s'' \in \{LOS, NLOS\}} \int_{R_1^{s''}(x)}^{\infty} \sum_{s' \in \{LOS, NLOS\}} (1 - \exp(Q^{s'}(y)) \Lambda_1^{s''}([0, y])) dy\right) \quad (21)$$

Proof. See Appendix E. ■

Due to the approximation used in deriving the analytical expression in theorem 4, its performance may degrade in some network configurations. For this reason, we propose an enhanced version of this approach that incorporates all $s'' \in \{LOS, NLOS\}$ holes that are outside of $B(0, D + R_1^{s''}(x))$ when the typical UE is associated with a $s \in \{LOS, NLOS\}$ BS in k^{th} tier (for more detail refer to Appendix E).

Corollary 2. *The coverage probability by incorporating all $s'' \in \{LOS, NLOS\}$ holes that are outside of $B(0, D + R_1^{s''}(x))$, when the typical UE is associated with a $s \in \{LOS, NLOS\}$ BS in k^{th} tier is*

$$P_C \approx \sum_{k=1}^2 \sum_{s \in \{LOS, NLOS\}} \sum_{n=1}^{v^s} (-1)^{n+1} \binom{v^s}{n} \int_0^{\infty} \exp(-\mu_{k,n}^s \sigma^2) \exp\left(-\sum_{j=1}^2 \sum_{s' \in \{LOS, NLOS\}} \{W_j^{s'}(x) + \Lambda_j^{s'}([0, R_j^{s'}(x)])\} \times T(x) \Lambda_k^s([0, x])\right) dx \quad (22)$$

where

$$T(x) = \exp\left(-\sum_{s'' \in \{LOS, NLOS\}} \int_{D+R_1^{s''}(x)}^{\infty} \sum_{s' \in \{LOS, NLOS\}} (1 - \exp(Q^{s'}(y)) \Lambda_1^{s''}([0, y])) dy\right) \quad (23)$$

We now move to the next section, where the accuracy of our approaches is evaluated by Monte Carlo simulations.

IV. NUMERICAL RESULTS

In this section, we evaluate the analytical expressions using numerical integration and validate the accuracy of the proposed expressions by comparing the simulation results. We assume MBSs and SBSs are operating at 28 GHz and the bandwidth assigned to each UE is $BW = 1$ GHz. Power path loss law are the same for both tiers, but different for LOS and NLOS links. The LOS probability function is $P^{LOS}(r) = \exp(-\beta r)$, where $\beta = \sqrt{2}/200$ [4], i.e. average LOS distance is 200 meters. Two different configurations similar to [13] are considered: low density and small holes (LD-SH) with $\lambda_1 = 2.5$ MBSs/km² and $D = 100$ meters, and high density and

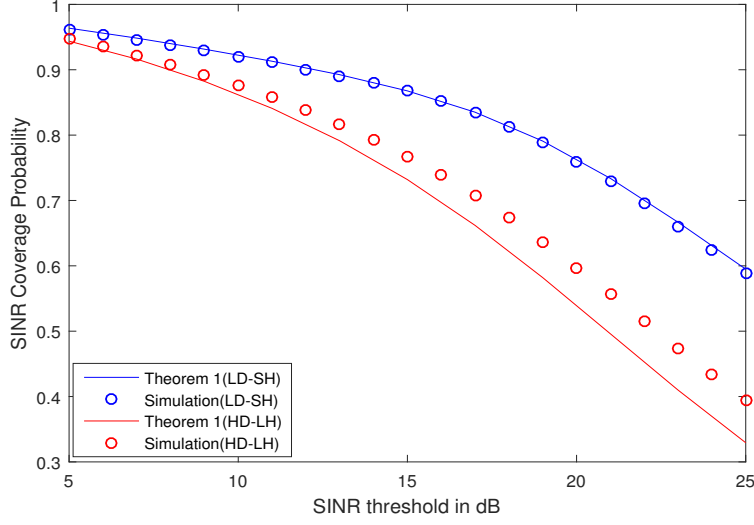


Fig. 2: SINR coverage probability as a function of SINR threshold-Theorem 1.

large holes (HD-LH) with $\lambda_1 = 10$ MBSs/km² and $D = 250$ meters. Also we have the following default values in our simulations:

- $M_k = M_{UE} = 10$ dB, $m_k = m_{UE} = -10$ dB and $\theta_k = \frac{\pi}{3}$, $\theta_{UE} = \frac{\pi}{2}$ as default value for main lobe array gain, side lobe array gain and beamwidth at BSs and UEs ($k = 1, 2$).
- Density of SBSs is $\lambda_2 = 20\lambda_1$ for all configurations.
- We set $\theta_c = \theta_1$ in all simulation.
- Path loss exponent values for LOS and NLOS links are $\alpha^{LOS} = 2$ and $\alpha^{NLOS} = 4$.
- $\sigma^2 = -174$ dBm/Hz + $10\log_{10}(\text{BW}) + 10$ dB.
- Transmission power for MBSs and SBSs are 53 dBm and 33 dBm respectively.
- The parameters of Nakagami fading for LOS and NLOS links are $v^{LOS} = 3$ and $v^{NLOS} = 2$.

First, we plot the analytical curves and the simulation results for the SINR coverage probability as a function of SINR threshold for all approaches in the two proposed configurations in Figs. 2 - 7. In these figures, blue and red circle marks represent the simulation results for LD-SH and HD-LH configurations respectively, and blue and red lines represent the analytical curves for LD-SH and HD-LH configurations respectively. In Fig. 2 the analytical expression for Theorem 1 in HD-LH configuration, where the effect of holes are significant, deviates from the simulation results. It reveals that PPP-based analytical result falls short of analyzing PHP distributed SBSs properly. Comparison between numerical results in Corollary 1 is shown in Fig. 3. As it can be

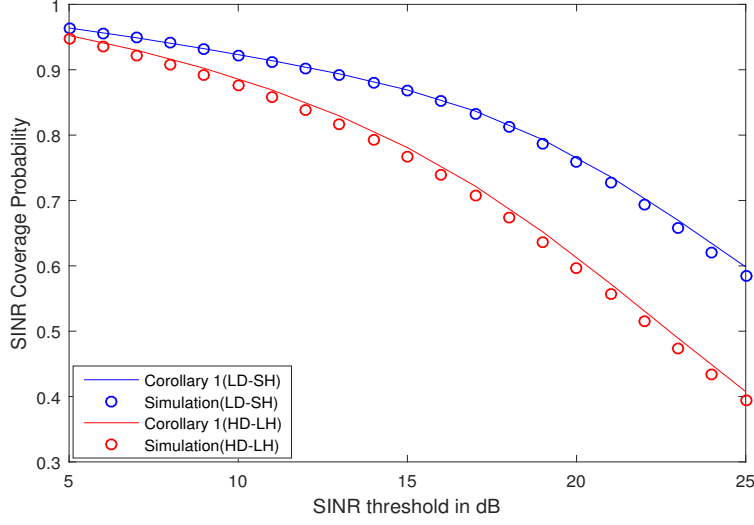


Fig. 3: SINR coverage probability as a function of SINR threshold-Corollary 1.

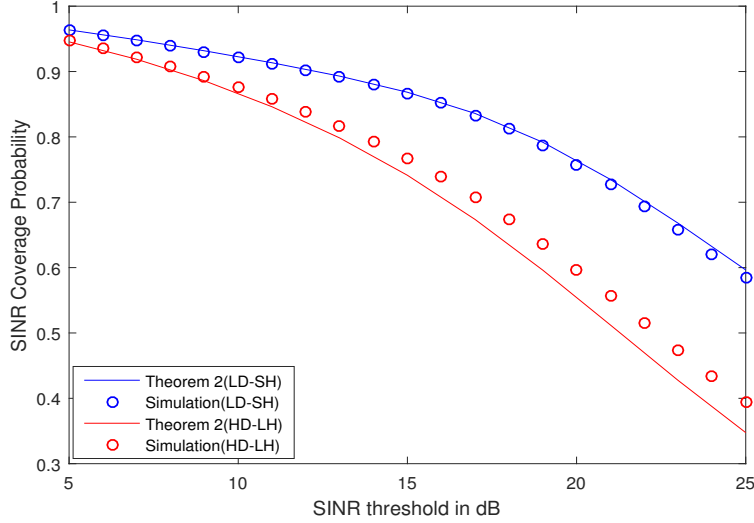


Fig. 4: SINR coverage probability as a function of SINR threshold-Theorem 2.

seen, this approximation works well even for HD-LH configuration. Note that we have used a modified PDF and association probability with λ_{PHP} in Corollary 1, which is a more accurate approximation than PPP-based PDF and the association probability [14].

Evaluating the coverage performance with considering the effect of the serving hole is shown in Fig. 4. The numerical results in Fig. 4 show that our analytical expressions in this theorem works better than Theorem 1 but still have some error. This is because we incorporate only a

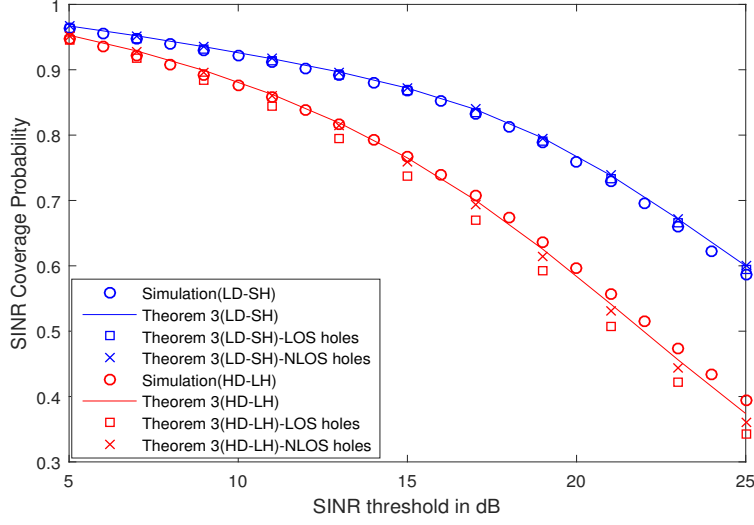


Fig. 5: SINR coverage probability as a function of SINR threshold-Theorem 3.

single hole when the typical UE is associated with an MBS. In Fig. 5 the analytical expression derived in Theorem 3 is compared with simulation result that confirms the accuracy of this approach. We also evaluated this theorem when incorporating only LOS/NLOS holes. Since exclusion radius of the interferer LOS MBSs is greater than NLOS MBSs in most cases, i.e. $R_1^{LOS}(x) \geq R_1^{NLOS}(x)$ for $x \geq 1$, incorporating only LOS holes have less effect on the coverage performance than incorporating only NLOS holes. Therefore, the results have lower coverage performance, when incorporating only LOS holes than when incorporating only NLOS holes.

Finally, the analytical curves in Theorem 4 are illustrated in Fig. 6. Similar to Fig. 5 evaluation of this approach, when incorporating only LOS/NLOS holes, is provided. Note that the performance gap between the analytical results and the simulation in HD-LH configuration have two reasons: First, in this case, overlaps between holes are ignored and therefore some points are removed multiple times. Second, we have ignored possible overlaps between incorporated holes and the exclusion region of the interferer SBSs (for more detail refer to Appendix E) and some non-existence points have been removed. To reduce the second effect in our analysis, we plot results given in Corollary 2 in Fig. 7. As expected, the coverage performance by incorporating all $s'' \in \{LOS, NLOS\}$ holes outside of $B(0, D + R_1^{s''}(x))$ have reduced. Actually, in this case, overlaps between holes and the exclusion region of the interferer SBSs have reduced and on the other hand, some near holes effect are ignored.

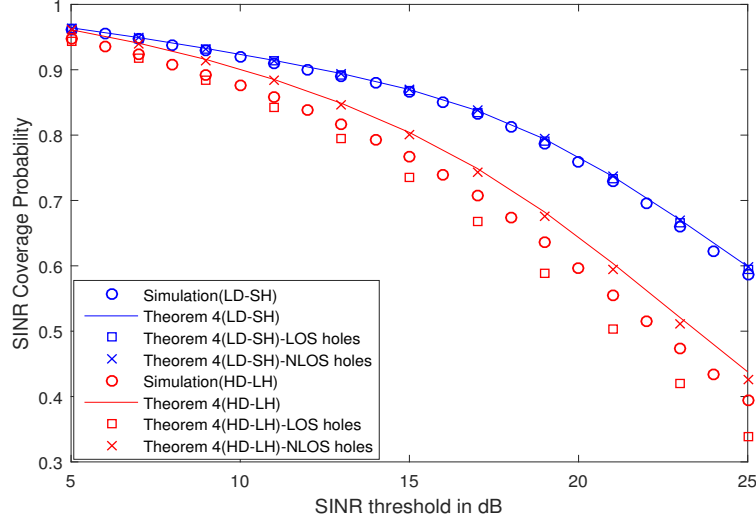


Fig. 6: SINR coverage probability as a function of SINR threshold-Theorem 4.

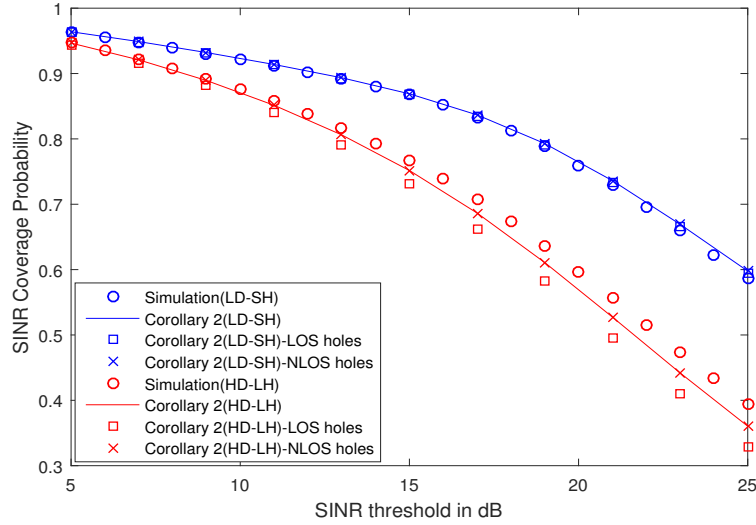


Fig. 7: SINR coverage probability as a function of SINR threshold-Corollary 2.

Since all results provide a remarkably accurate characterization of the coverage probability in LD-SH configuration, we study only HD-LH configuration in the next figures, which is the most challenging configuration for evaluating the analytical expressions. In Fig. 8, the coverage probability of the typical UE is plotted by varying the hole radius. Since the analytical expression in Theorem 1 is independent of the hole radius, results are exactly the same for different values of D . Comparison of the other proposed results with the simulations reveal that even in HD-LH

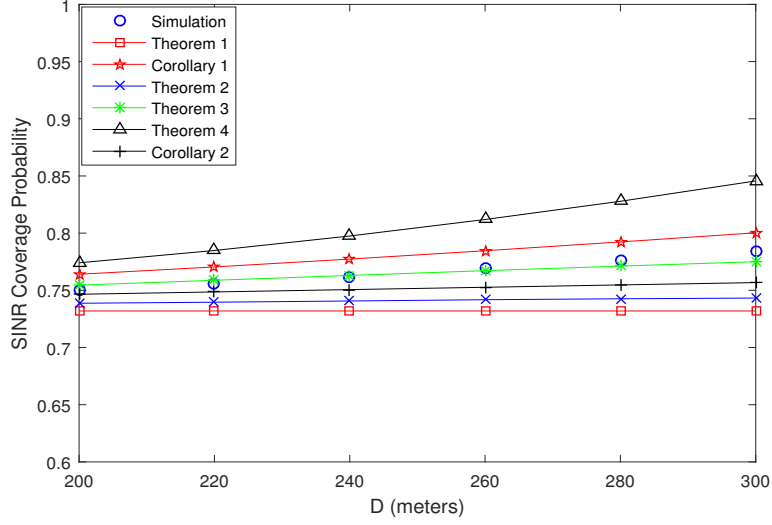


Fig. 8: SINR coverage probability as a function of hole radius. ($\lambda_1 = 10$ MBSs/km²)

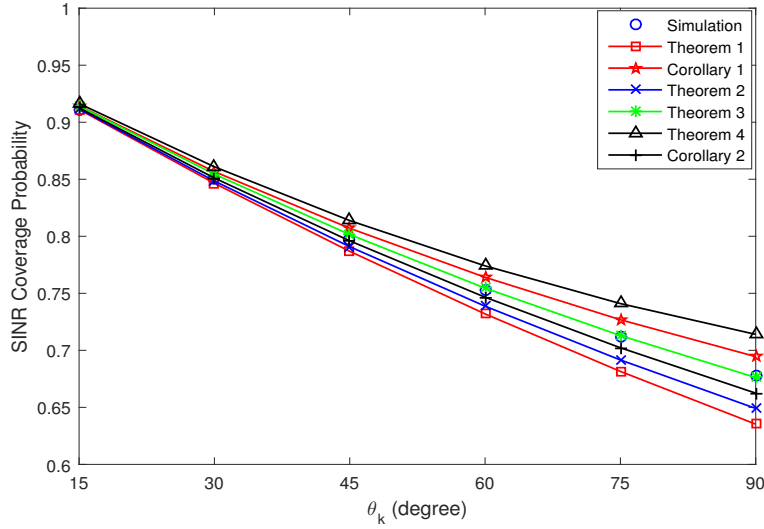


Fig. 9: SINR coverage probability as a function of BS beamwidth. ($\lambda_1 = 10$ MBSs/km², $D = 200$ meters)

configuration all of them have better performance than PPP-based analysis. Next, we plot the coverage probability as a function of the beamwidth of BSs (both MBSs and SBSs) in Fig. 9. Note that by increasing antenna beamwidth, more BSs will transmit interference signals to the typical UE via their main lobes, which results in a larger interference power and a weaker coverage. Since by increasing beamwidth, we increase the central angle of circular sector holes

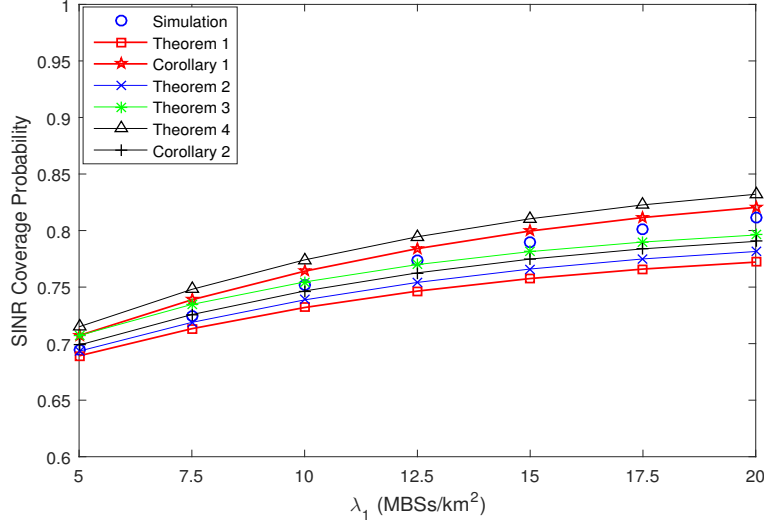


Fig. 10: SINR coverage probability as a function of MBSs density. ($D = 200$ meters)

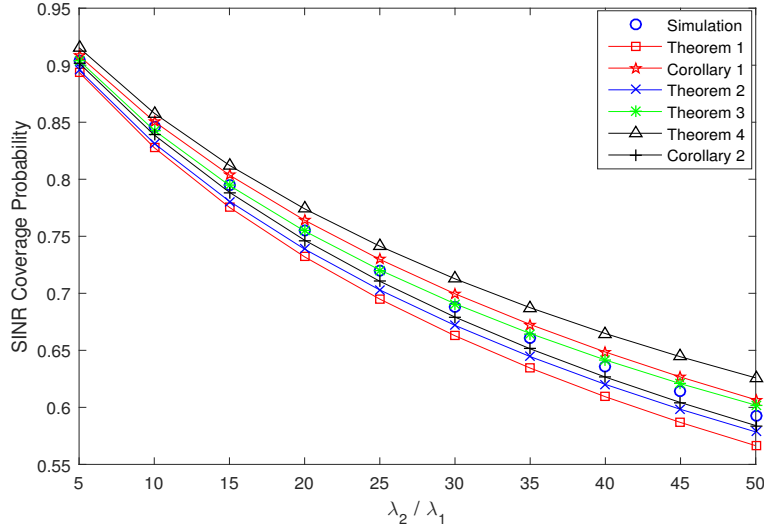


Fig. 11: SINR coverage probability as a function of λ_2/λ_1 . ($\lambda_1 = 10$ MBSs/km², $D = 200$ meters)

simultaneously, overlaps between holes are more significant. Nonetheless, Fig. 9 shows that even with increasing antenna beamwidth all proposed approaches have reliable performances. Fig. 10 shows the effect of MBSs density on the coverage probability. Small values of λ_1 result in LD-LH configuration, whereas high values result in HD-LH configuration. Finally, we plot the coverage probability as a function of λ_2/λ_1 in Fig. 11. As was the case in the above results, all proposed analytical expressions work well with a minor error compared to the simulation result

in HD-LH configuration and provide better analysis than Theorem 1.

V. CONCLUSION

In this paper, we have provided an analytical framework to compute the SINR coverage probability in the downlink of a mmWave two-tier HCN with spatial separation between tiers. Due to fundamental physical differences between mmWave and microwave propagation, we used directional beamforming, a blockage model and Nakagami fading to incorporate these differences. Prior works in mmWave HCNs focus on modeling the location of BSs as homogeneous independent PPPs to capture the irregular network topology. To provide more realistic network model, we considered spatial separation between tiers by modeling the location of SBSs as a PHP. Since the interference characterization in deriving the SINR coverage probability is difficult, we have used some approximations. Then analytical expression for SINR coverage probability have been derived using different approaches and compared with the simulation results. Numerical results show a dramatic improvement in the accuracy of our proposed approaches with that of the prior PPP-based analysis for mmWave HCN. Moreover, we have used circular sector hole in our analysis that is different from the prior PHP models, i.e, the circular region as default shape for holes. It should be noted that analysis based on this hole configuration can be simply extended to the circular hole and is an exciting point for proposing different shapes of the hole in PHP. It would be an interesting topic to analyze the hybrid networks with overlaid microwave macrocells as a future work. Providing an accurate analysis of the capacity-centric deployments in mmWave HCNs using other point processes, such as PCP and MCP, is another promising direction for future work.

APPENDIX

A. Proof of Lemma 2

Based on the proposed cell association rule, the typical UE is associated with a $s \in \{LOS, NLOS\}$ BS in k^{th} tier if the following is satisfied

$$\begin{aligned} P_k G_k r_k^{-\alpha^s} &> P_j G_j r_j^{-\alpha^{s'}} \stackrel{a}{=} P_k M_k M_{UE} r_k^{-\alpha^s} > P_j M_j M_{UE} r_j^{-\alpha^{s'}} \\ &= P_k M_k r_k^{-\alpha^s} > P_j M_j r_j^{-\alpha^{s'}} = r_j > \left(\frac{P_j}{P_k} \times \frac{M_j}{M_k}\right)^{1/\alpha^{s'}} \times r_k^{\alpha^s/\alpha^{s'}} \end{aligned} \quad (24)$$

where (a) follows by the serving link directivity gain assumption and $j = 1, 2, s' \in \{LOS, NLOS\}$.

Let us denote the serving tier and LOS or NLOS state of BSs by T and S , respectively. Now we calculate $Pr(T = k, S = s | r_k = x)$ by ignoring holes. Note that it is possible that the typical UE observes no $s \in \{LOS, NLOS\}$ BS in ϕ_1^s and ψ^s [4]. The typical UE is associated with a $s \in \{LOS, NLOS\}$ BS in k^{th} tier if and only if it has a $s \in \{LOS, NLOS\}$ BS in that tier, and its nearest BS in k^{th} tier has smaller average power than that of the nearest $s' \neq s$ BS in k^{th} tier and the nearest $s' \in \{LOS, NLOS\}$ BS in $j \neq k$ tier. Hence, it follows that

$$\begin{aligned} Pr(T = k, S = s | r_k = x) &= Pr(r_k > x^{\alpha^s/\alpha^{s'}}, s' \neq s) Pr(r_j > R_j^{s'}(x), j \neq k, s' \in \{LOS, NLOS\}) \\ &= exp(-\Lambda_k^{s'}([0, x^{\alpha^s/\alpha^{s'}}])) exp(-\sum_{s' \in \{LOS, NLOS\}} \Lambda_j^{s'}([0, R_j^{s'}(x)])) \end{aligned} \quad (25)$$

Therefore, A_k^s can be expressed as

$$\begin{aligned} A_k^s &= B_k^s Pr(T = k, S = s) = B_k^s \mathbb{E}_x[Pr(T = k, S = s | r_k = x)] \\ &= B_k^s \int_0^\infty exp(-\Lambda_k^{s'}([0, x^{\alpha^s/\alpha^{s'}}])) exp(-\sum_{s' \in \{LOS, NLOS\}} \Lambda_j^{s'}([0, R_j^{s'}(x)])) f_k^s(r_k = x) dx \\ &= \int_0^\infty \Lambda_k^{s'}([0, x]) exp(-\sum_{j=1}^2 \sum_{s' \in \{LOS, NLOS\}} \Lambda_j^{s'}([0, R_j^{s'}(x)])) dx \end{aligned} \quad (26)$$

B. Proof of Theorem 1

SINR coverage probability is

$$P_C = Pr(SINR > \tau_k) \stackrel{a}{=} \sum_{k=1}^2 \sum_{s \in \{LOS, NLOS\}} A_k^s P_{C_k}^s(\tau_k) \quad (27)$$

where (a) follows from total probability law and $P_{C_k}^s(\tau_k)$ is the conditional coverage probability given that the typical UE is associated with a $s \in \{LOS, NLOS\}$ BS in k^{th} tier. A_k^s is the association probability provided in Lemma 2. $P_{C_k}^s(\tau_k)$ is calculated as follows

$$\begin{aligned} P_{C_k}^s(\tau_k) &= Pr(SINR > \tau_k | T = k, S = s) = \mathbb{E}_x[Pr(SINR > \tau_k | T = k, S = s, r_k = x)] \\ &= \int_0^\infty Pr(SINR > \tau_k | T = k, S = s, r_k = x) \times f(r_k = x | T = k, S = s) dx \end{aligned} \quad (28)$$

$f(r_k = x \mid T = k, S = s)$ is the conditional PDF of the distance between the closest BS and the typical UE, when the typical UE is associated with a $s \in \{LOS, NLOS\}$ BS in k^{th} tier. This PDF can be calculated as follows

$$\begin{aligned} f(r_k = x \mid T = k, S = s) &\stackrel{a}{=} \frac{Pr(T = k, S = s, \mid r_k = x) f^s(r_k = x)}{Pr(T = k, S = s)} \\ &\stackrel{b}{=} \frac{1}{A_k^s} \Lambda_k^s([0, x)) \exp\left(-\sum_{j=1}^2 \sum_{s' \in \{LOS, NLOS\}} \Lambda_j^{s'}([0, R_j^{s'}(x)))\right) \end{aligned} \quad (29)$$

where (a) follows from the Bayes theorem and (b) from equation (25) in Appendix A .

In order to complete our derivation for SINR coverage probability, we derive $Pr(SINR > \tau_k \mid T = k, S = s, r_k = x)$

$$Pr(SINR > \tau_k \mid T = k, S = s, r_k = x) = Pr(SINR_k^s > \tau_k \mid r_k = x) \quad (30)$$

where $SINR_k^s$ was defined in equation (8). Therefore, we have

$$\begin{aligned} Pr(SINR_k^s > \tau_k \mid r_k = x) &= Pr\left(\frac{P_k |h_{k,0}|^2 G_{k,0} x^{-\alpha^s}}{\sigma^2 + I} > \tau_k\right) \\ &= Pr(|h_{k,0}|^2 > \frac{\tau_k(\sigma^2 + I)}{P_k G_{k,0} x^{-\alpha^s}}) \stackrel{a}{\approx} \sum_{n=1}^{v^s} (-1)^{n+1} \binom{v^s}{n} \mathbb{E}[\exp(-\mu_{k,n}^s \sigma^2)] \mathbb{E}[\exp(-\mu_{k,n}^s I)] \end{aligned} \quad (31)$$

where $\mu_{k,n}^s$ was defined in Theorem 1 and step (a) follows similar approach used in [4], which is an upper bound for CCDF of gamma random variable with parameter v^s . In order to calculate $\mathbb{E}[\exp(-\mu_{k,n}^s I)]$, we define I as following

$$\begin{aligned} I &= \sum_{s' \in \{LOS, NLOS\}} \sum_{i \in \{\phi_1^{s'}\} \setminus BS_{k,0}} P_1 |h_{1,i}|^2 G_{1,i} r_{1,i}^{-\alpha^{s'}} + \sum_{s' \in \{LOS, NLOS\}} \sum_{i \in \{\psi^{s'}\} \setminus BS_{k,0}} P_2 |h_{2,i}|^2 G_{2,i} r_{2,i}^{-\alpha^{s'}} \\ &= \sum_{j=1}^2 \sum_{s' \in \{LOS, NLOS\}} \sum_{i \in \{\phi_j^{s'}\} \setminus BS_{k,0}} P_j |h_{j,i}|^2 G_{j,i} r_{j,i}^{-\alpha^{s'}} - \sum_{s' \in \{LOS, NLOS\}} \sum_{i \in \{\phi_2^{s'} \cap \psi^{s'c}\}} P_2 |h_{2,i}|^2 G_{2,i} r_{2,i}^{-\alpha^{s'}} \end{aligned} \quad (32)$$

Let us denote

$$I_H = \sum_{s' \in \{LOS, NLOS\}} \sum_{i \in \{\phi_2^{s'} \cap \psi^{s'c}\}} P_2 |h_{2,i}|^2 G_{2,i} r_{2,i}^{-\alpha^{s'}} \quad (33)$$

which represents the interference from SBSs of the baseline PPP ϕ_2 who are inside of holes.

Since in this approach, PHP distribution of SBSs (ψ) is approximated by the baseline PPP, ϕ_2 , $I_H = 0$. Hence, we have

$$\begin{aligned}
\mathbb{E}[\exp(-\mu_{k,n}^s I)] &= \mathbb{E}[\exp(-\mu_{k,n}^s (\sum_{j=1}^2 \sum_{s' \in \{LOS, NLOS\}} \sum_{i \in \{\phi_j^{s'}\}} P_j |h_{j,i}|^2 G_{j,i} r_{j,i}^{-\alpha^{s'}})))] \\
&\stackrel{a}{=} \prod_{j=1}^2 \prod_{s' \in \{LOS, NLOS\}} \mathbb{E}[\prod_{i \in \{\phi_j^{s'}\} \setminus BS_{k,0}} \exp(-\mu_{k,n}^s P_j |h_{j,i}|^2 G_{j,i} r_{j,i}^{-\alpha^{s'}})] \\
&\stackrel{b}{=} \prod_{j=1}^2 \prod_{s' \in \{LOS, NLOS\}} \exp(-\int_{R_j^{s'}(x)}^{\infty} (1 - \mathbb{E}[\exp(-\mu_{k,n}^s P_j |h_j|^2 G_j r^{-\alpha^{s'}})]) A_j'^{s'}([0, r]) dr)
\end{aligned} \tag{34}$$

where step (a) is due to the independence assumption among tiers and LOS/NLOS BSs in each tier and (b) follows from the probability generating functional (PGFL) of a PPP. The integration range excludes a ball centered at 0 and radius $R_j^{s'}(x) = (\frac{P_j}{P_k} \times \frac{M_j}{M_k})^{1/\alpha^{s'}} \times x^{\alpha^s/\alpha^{s'}}$ because the closest $s' \in \{LOS, NLOS\}$ interferer in j^{th} tier has to be farther than the serving BS, based on cell association rule considered. In the next step we need to calculate $\mathbb{E}[\exp(-\mu_{k,n}^s (P_j |h_j|^2 G_j r^{-\alpha^{s'}}))]$

$$\begin{aligned}
\mathbb{E}[\exp(-\mu_{k,n}^s P_j |h_j|^2 G_j r^{-\alpha^{s'}})] &\stackrel{a}{=} \sum_{g=1}^4 P_{j,g} \mathbb{E}_{|h_j|^2} [\exp(-\mu_{k,n}^s P_j |h_j|^2 A_{j,g} r^{-\alpha^{s'}})] \\
&\stackrel{b}{=} \sum_{g=1}^4 P_{j,g} \left(\frac{1}{1 + (\mu_{k,n}^s P_j A_{j,g} r^{-\alpha^{s'}})/v^{s'}} \right)^{v^{s'}}
\end{aligned} \tag{35}$$

where in (a) expectation are taken over G_j , $P_{j,g}$ and $A_{j,g}$ are constants defined in Table II, and step (b) follows from computing the moment generating function of the gamma distributed random variable $|h_j|^2$. Finally, by combining (35), (34), (31), (28) and (27), SINR coverage probability expression given in Theorem 1 is obtained.

C. Proof of Theorem 2

In the case of incorporating the serving hole, we follow the same approach used in Appendix B and equation (27)-(31) are held in this proof too. It is enough to consider the effect of the serving hole in the interference characterization. Therefore, we approximate I as following, which incorporates the serving hole and ignores other holes

$$\begin{aligned}
I &= \sum_{s' \in \{LOS, NLOS\}} \sum_{i \in \{\phi_1^{s'}\} \setminus BS_{k,0}} P_1 |h_{1,i}|^2 G_{1,i} r_{1,i}^{-\alpha^{s'}} + \\
&\quad \sum_{s' \in \{LOS, NLOS\}} \sum_{i \in \{\psi^{s'} \cap S^c(x, D, \theta_c)\} \setminus BS_{k,0}} P_2 |h_{2,i}|^2 G_{2,i} r_{2,i}^{-\alpha^{s'}}
\end{aligned} \tag{36}$$

where $S(x, D, \theta_c)$ was defined in Definition 1 and x is the distance between the serving MBS and the typical UE. Now we calculate $\mathbb{E}[\exp(-\mu_{k,n}^s I)]$

$$\begin{aligned}
& \mathbb{E}[\exp(-\mu_{k,n}^s I)] \\
&= \mathbb{E}[\exp(-\mu_{k,n}^s (\sum_{s' \in \{LOS, NLOS\}} \sum_{i \in \{\phi_1^{s'}\} \setminus BS_{k,0}} P_1 |h_{1,i}|^2 G_{1,i} r_{1,i}^{-\alpha^{s'}} + \\
&\quad \sum_{s' \in \{LOS, NLOS\}} \sum_{i \in \{\psi^{s'} \cap S^c(x, D, \theta_c)\} \setminus BS_{k,0}} P_2 |h_{2,i}|^2 G_{2,i} r_{2,i}^{-\alpha^{s'}}))] \\
&\stackrel{a}{=} \prod_{s' \in \{LOS, NLOS\}} \mathbb{E}[\prod_{i \in \{\phi_1^{s'}\} \setminus BS_{k,0}} \exp(-\mu_{k,n}^s P_1 |h_{1,i}|^2 G_{1,i} r_{1,i}^{-\alpha^{s'}})] \\
&\quad \prod_{s' \in \{LOS, NLOS\}} \mathbb{E}[\prod_{i \in \{\psi^{s'} \cap S^c(x, D, \theta_c)\} \setminus BS_{k,0}} \exp(-\mu_{k,n}^s P_2 |h_{2,i}|^2 G_{2,i} r_{2,i}^{-\alpha^{s'}})] \\
&\stackrel{b}{=} \prod_{s' \in \{LOS, NLOS\}} \exp(-\int_{R_1^{s'}(x)}^{\infty} (1 - \mathbb{E}[\exp(-\mu_{k,n}^s P_1 |h_1|^2 G_1 r^{-\alpha^{s'}})]) A_1^{s'}([0, r]) dr) \\
&\quad \prod_{s' \in \{LOS, NLOS\}} \exp(-\int_{R_2^{s'}(x)}^{\infty} (1 - \mathbb{E}[\exp(-\mu_{k,n}^s P_2 |h_2|^2 G_2 r^{-\alpha^{s'}})]) A_2^{s'}([0, r]) dr) \\
&\quad \prod_{s' \in \{LOS, NLOS\}} \exp(\lambda_2 \int_{\Xi} (1 - \mathbb{E}[\exp(-\mu_{1,n}^s P_2 |h_2|^2 G_2 r^{-\alpha^{s'}})]) P^{s'}(r) dS) \\
&= \prod_{j=1}^2 \prod_{s' \in \{LOS, NLOS\}} \exp(-\int_{R_j^{s'}(x)}^{\infty} (1 - \mathbb{E}[\exp(-\mu_{k,n}^s P_j |h_j|^2 G_j r^{-\alpha^{s'}})]) A_j^{s'}([0, r]) dr) \\
&\quad \prod_{s' \in \{LOS, NLOS\}} \exp(\lambda_2 \int_{\Xi} (1 - \mathbb{E}[\exp(-\mu_{1,n}^s P_2 |h_2|^2 G_2 r^{-\alpha^{s'}})]) P^{s'}(r) dS)
\end{aligned} \tag{37}$$

where (a) is due to the independence assumption among tiers and LOS/NLOS BSs in each tier and (b) follows from the PGFL of a PPP. $\Xi = S(x, D, \theta_c) \cap B^c(0, R_2^{s'}(x))$ and $B^c(0, R_2^{s'}(x))$ represents regions that are outside of a ball centered at the origin with radius $R_2^{s'}(x) = (\frac{P_2}{P_k} \times \frac{M_2}{M_k})^{1/\alpha^{s'}} \times x^{\alpha^s/\alpha^{s'}}$.

Next, we need to calculate $\int_{\Xi} (1 - \mathbb{E}[\exp(-\mu_{1,n}^s P_2 |h_2|^2 G_2 r^{-\alpha^{s'}})]) P^{s'}(r) dS$. For this, we use transformation as below

$$r = \sqrt{u^2 + x^2 - 2ux \cos(\phi)} \tag{38}$$

where the above equation is derived based on cosine-law, u and ϕ is defined in Fig. 12.

To maintain tractability, we approximate $\Xi \approx S(x, D, \theta_c)$. It is possible to consider exact region in calculating the integral, but it leads to a complex analytical expression, hence,

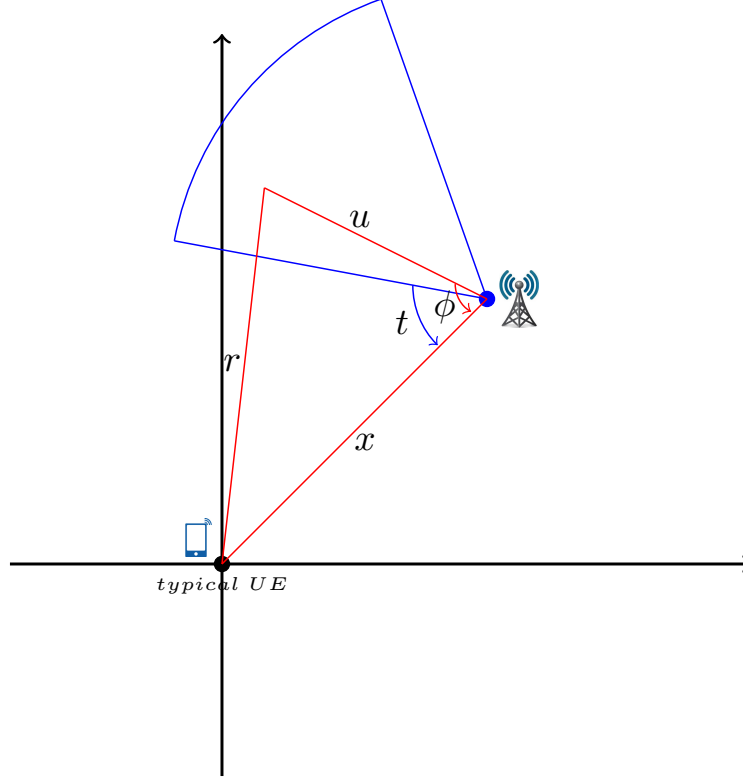


Fig. 12: Illustration of the effect of a hole in the interference characterization.

we use the approximated region instead of the exact one. Due to this assumptions, $\int_{\Xi}(1 - \mathbb{E}[\exp(-\mu_{1,n}^s P_2 |h_2|^2 G_2 r^{-\alpha^{s'}})]) P^{s'}(r) dS$ can be evaluated as

$$\begin{aligned} & \int_{\Xi} (1 - \mathbb{E}[\exp(-\mu_{1,n}^s P_2 |h_2|^2 G_2 r^{-\alpha^{s'}})]) P^{s'}(r) dS \\ & \approx \int_t^{t+\theta_c} \int_0^D (1 - \mathbb{E}[\exp(-\mu_{1,n}^s P_j |h_2|^2 G_2 (u^2 + x^2 - 2ux\cos(\phi))^{-\alpha^{s'}/2})]) \\ & P^{s'}(\sqrt{u^2 + x^2 - 2ux\cos(\phi)}) u du d\phi \end{aligned} \quad (39)$$

Since the direction of circular sectors have a uniform distribution in $[0, 2\pi)$, we have

$$\begin{aligned} & \int_{\Xi} (1 - \mathbb{E}[\exp(-\mu_{1,n}^s P_2 |h_2|^2 G_2 r^{-\alpha^{s'}})]) P^{s'}(r) dS \\ & \approx \int_0^{2\pi} \int_t^{t+\theta_c} \int_0^D (1 - \mathbb{E}[\exp(-\mu_{1,n}^s P_j |h_2|^2 G_2 (u^2 + x^2 - 2ux\cos(\phi))^{-\alpha^{s'}/2})]) \\ & P^{s'}(\sqrt{u^2 + x^2 - 2ux\cos(\phi)}) \frac{1}{2\pi} u du d\phi dt \\ & \stackrel{a}{=} \frac{\theta_c}{2\pi} \int_0^{2\pi} \int_0^D (1 - \mathbb{E}[\exp(-\mu_{1,n}^s P_j |h_2|^2 G_2 (u^2 + x^2 - 2ux\cos(\phi))^{-\alpha^{s'}/2})]) \\ & P^{s'}(\sqrt{u^2 + x^2 - 2ux\cos(\phi)}) u du d\phi \end{aligned} \quad (40)$$

where (a) is derived by substituting integrals and using this fact that integrand function is periodic respect to ϕ with period 2π .

Using similar approach in equation (35) to derive $\mathbb{E}[\exp(-\mu_{1,n}^s P_2 |h_2|^2 G_2 (u^2 + x^2 - 2ux \cos(\phi))^{-\alpha^{s'}/2})]$, SINR coverage probability by incorporating serving hole can be expressed as Theorem 2.

D. Proof of Theorem 3

Similar to the proof used in Appendix C, the approximation of the interference in this case is

$$I = \sum_{s' \in \{LOS, NLOS\}} \sum_{i \in \{\phi_1^{s'}\} \setminus BS_{k,0}} P_1 |h_{1,i}|^2 G_{1,i} r_{1,i}^{-\alpha^{s'}} + \sum_{s' \in \{LOS, NLOS\}} \sum_{i \in \{\psi^{s'} \cap \Omega^c\} \setminus BS_{k,0}} P_2 |h_{2,i}|^2 G_{2,i} r_{2,i}^{-\alpha^{s'}} \quad (41)$$

where $\Omega = \bigcup_{s'' \in \{LOS, NLOS\}} S(y, D, \theta_c)$ and y is the distance between $s'' \in \{LOS, NLOS\}$ interferer MBS and the typical UE. We ignore possible overlaps between two holes and approximate Ω as $\Omega \approx \sum_{s'' \in \{LOS, NLOS\}} S(y, D, \theta_c)$. Similar to equation (37), $\mathbb{E}[\exp(-\mu_{k,n}^s I) | y]$ is

$$\begin{aligned} & \mathbb{E}[\exp(-\mu_{k,n}^s I) | y] \\ &= \prod_{j=1}^2 \prod_{s' \in \{LOS, NLOS\}} \exp\left(-\int_{R_j^{s'}(x)}^{\infty} (1 - \mathbb{E}[\exp(-\mu_{k,n}^s P_j |h_j|^2 G_j r^{-\alpha^{s'}})]) A_j^{s'}([0, r] dr)\right) \\ & \quad \prod_{s' \in \{LOS, NLOS\}} \exp\left(\lambda_2 \int_{\Omega} (1 - \mathbb{E}[\exp(-\mu_{k,n}^s P_2 |h_2|^2 G_2 r^{-\alpha^{s'}})]) P^{s'}(r) dS\right) \end{aligned} \quad (42)$$

Note that the exact region for the integral is $\Omega \cap B^c(0, R_2^{s'}(x))$, but we approximate it by Ω . Similar to proof in Appendix C, $\int_{\Omega} (1 - \mathbb{E}[\exp(-\mu_{k,n}^s P_2 |h_2|^2 G_2 r^{-\alpha^{s'}})]) P^{s'}(r) dS$ can be calculated as below

$$\begin{aligned} & \int_{\Omega} (1 - \mathbb{E}[\exp(-\mu_{k,n}^s P_2 |h_2|^2 G_2 r^{-\alpha^{s'}})]) P^{s'}(r) dS \\ & \approx \sum_{s'' \in \{LOS, NLOS\}} \frac{\theta_c}{2\pi} \int_0^{2\pi} \int_0^D (1 - \mathbb{E}[\exp(-\mu_{k,n}^s P_2 |h_2|^2 G_2 (u^2 + y^2 - 2uy \cos(\phi))^{-\alpha^{s'}/2})]) \\ & \quad P^{s'}(\sqrt{u^2 + y^2 - 2uy \cos(\phi)}) u du d\phi \end{aligned} \quad (43)$$

Now, to complete our derivation, we need to calculate PDF of y . Given that the typical UE is associated with a $s \in \{LOS, NLOS\}$ BS in k^{th} tier at distance $r_k = x$ and observes at least one $s'' \in \{LOS, NLOS\}$ MBS, CCDF of y is

$$\begin{aligned}\bar{F}^{s''}(y|T = k, S = s, r_k = x) &= Pr(Y > y|T = k, S = s, r_k = x) \\ &= Pr(\mathbb{N}(B(0, y) \setminus B(0, R_1^{s''}(x))) = \emptyset) = \frac{\exp(-\Lambda_1^{s''}([0, y]))\exp(\Lambda_1^{s''}([0, R_1^{s''}(x)]))}{1 - \exp(-\Lambda_1([R_1^{s''}(x), \infty)))}\end{aligned}\quad (44)$$

where \mathbb{N} represents the number of points in ϕ_1 that are in the desired set and $R_1^{s''}(x)$ is defined in Theorem 3. PDF of y now follows by differentiating the above expression

$$\begin{aligned}f^{s''}(y|T = k, S = s, r_k = x) &= -\frac{d}{dy}\bar{F}^{s''}(y|T = k, S = s, r_k = x) \\ &= \frac{\Lambda_1^{s''}([0, y])\exp(-\Lambda_1^{s''}([0, y]) + \Lambda_1^{s''}([0, R_1^{s''}(x)]))}{1 - \exp(-\Lambda_1([R_1^{s''}(x), \infty)))}\end{aligned}\quad (45)$$

Finally $\mathbb{E}[\exp(-\mu_{k,n}^s I)]$ can be expressed as

$$\begin{aligned}\mathbb{E}[\exp(-\mu_{k,n}^s I)] &= \prod_{j=1}^2 \prod_{s' \in \{LOS, NLOS\}} \exp\left(-\int_{R_j^{s'}(x)}^{\infty} (1 - \mathbb{E}[\exp(-\mu_{k,n}^s P_j |h_j|^2 G_j r^{-\alpha^{s'}})]) \Lambda_j^{s'}([0, r]) dr\right) \\ &\quad \prod_{s' \in \{LOS, NLOS\}} \prod_{s'' \in \{LOS, NLOS\}} \int_{R_1^{s''}(x)}^{\infty} \exp\left(\frac{\theta_c}{2\pi} \lambda_2 \int_0^{2\pi} \int_0^D (1 - \mathbb{E}[\exp(-\mu_{k,n}^s P_2 |h_2|^2 G_2 (u^2 + y^2 - 2uy\cos(\phi))^{-\alpha^{s'}/2}]]) \right. \\ &\quad \left. P^{s'}(\sqrt{u^2 + y^2 - 2uy\cos(\phi)}) udud\phi\right) f^{s''}(y|T = k, S = s, r_k = x) dy\end{aligned}\quad (46)$$

Similar to equation (35), $\mathbb{E}[\exp(-\mu_{k,n}^s P_j |h_j|^2 G_j r^{-\alpha^{s'}})]$ and $\mathbb{E}[\exp(-\mu_{k,n}^s P_2 |h_2|^2 G_2 (u^2 + y^2 - 2uy\cos(\phi))^{-\alpha^{s'}/2})]$ can be calculated. Therefore, SINR coverage probability by incorporating the nearest non-serving LOS and NLOS can be obtained.

E. Proof of Theorem 4

The exact expression for the interference in our proposed two-tier HCN model is

$$I = \sum_{s' \in \{LOS, NLOS\}} \sum_{i \in \{\phi_1^{s'}\} \setminus BS_{k,0}} P_1 |h_{1,i}|^2 G_{1,i} r_{1,i}^{-\alpha^{s'}} + \sum_{s' \in \{LOS, NLOS\}} \sum_{i \in \{\phi_2^{s'} \cap \Gamma^c\} \setminus BS_{k,0}} P_2 |h_{2,i}|^2 G_{2,i} r_{2,i}^{-\alpha^{s'}}\quad (47)$$

where $\Gamma = \bigcup_{y \in \phi_1} S(y, D, \theta_c)$. However, due to the possible overlaps between the holes, the exact characterization of I is complex. Therefore, we approximate Γ as $\Gamma \approx \sum_{s'' \in \{LOS, NLOS\}} \sum_{y \in \phi_1^{s''}} S(y, D, \theta_c)$,

which ignores possible overlaps between the holes and provide an upper bound for the interference. Using this assumption $\mathbb{E}[\exp(-\mu_{k,n}^s I)]$ can be evaluated as

$$\begin{aligned}
& \mathbb{E}[\exp(-\mu_{k,n}^s I)] \\
& \approx \prod_{j=1}^2 \prod_{s' \in \{LOS, NLOS\}} \exp\left(-\int_{R_j^{s'}(x)}^{\infty} (1 - \mathbb{E}[\exp(-\mu_{k,n}^s P_j | h_j|^2 G_j r^{-\alpha^{s'}})]) \Lambda_j^{s'}([0, r) dr\right) \\
& \quad \prod_{s' \in \{LOS, NLOS\}} \mathbb{E}_{\phi_1} \left[\exp\left(\lambda_2 \int_{\Gamma} (1 - \mathbb{E}[\exp(-\mu_{k,n}^s P_2 | h_2|^2 G_2 r^{-\alpha^{s'}})]) P^{s'}(r) dS\right) \right] \\
& \approx \exp\left(-\sum_{j=1}^2 \sum_{s' \in \{LOS, NLOS\}} W_j^{s'}(x)\right) \prod_{s' \in \{LOS, NLOS\}} \\
& \quad \mathbb{E}_{\phi_1^{s''}} \left[\exp\left(\sum_{s'' \in \{LOS, NLOS\}} \sum_{y \in \phi_1^{s''}} \lambda_2 \int_{S(y, D, \theta_c)} (1 - \mathbb{E}[\exp(-\mu_{k,n}^s P_2 | h_2|^2 G_2 r^{-\alpha^{s'}})]) P^{s'}(r) dS\right) \right] \\
& \approx \exp\left(-\sum_{j=1}^2 \sum_{s' \in \{LOS, NLOS\}} W_j^{s'}(x)\right) \prod_{s' \in \{LOS, NLOS\}} \prod_{s'' \in \{LOS, NLOS\}} \\
& \quad \mathbb{E}_{\phi_1^{s''}} \left[\prod_{y \in \phi_1^{s''}} \exp\left(\lambda_2 \int_{S(y, D, \theta_c)} (1 - \mathbb{E}[\exp(-\mu_{k,n}^s P_2 | h_2|^2 G_2 r^{-\alpha^{s'}})]) P^{s'}(r) dS\right) \right] \\
& \approx \exp\left(-\sum_{j=1}^2 \sum_{s' \in \{LOS, NLOS\}} W_j^{s'}(x)\right) \prod_{s' \in \{LOS, NLOS\}} \prod_{s'' \in \{LOS, NLOS\}} \\
& \quad \exp\left(-\int_{R_1^{s''}(x)}^{\infty} (1 - \exp(\lambda_2 \int_{S(y, D, \theta_c)} (1 - \mathbb{E}[\exp(-\mu_{k,n}^s P_2 | h_2|^2 G_2 r^{-\alpha^{s'}})]) P^{s'}(r) dS)) \Lambda_1^{s''}([0, y)) dy\right) \\
& \approx \exp\left(-\sum_{j=1}^2 \sum_{s' \in \{LOS, NLOS\}} W_j^{s'}(x)\right) \\
& \quad \exp\left(-\sum_{s'' \in \{LOS, NLOS\}} \int_{R_1^{s''}(x)}^{\infty} \sum_{s' \in \{LOS, NLOS\}} (1 - \exp(Q^{s'}(y))) \Lambda_1^{s''}([0, y)) dy\right)
\end{aligned} \tag{48}$$

Note that similar to prior proofs, the exact region for the integral is $\Gamma \cap B^c(0, R_2^{s'}(x))$, but we approximate it by Γ .

REFERENCES

- [1] J. G. Andrews, S. Buzzi, W. Choi, S. V. Hanly, A. Lozano, A. C. K. Soong, and J. C. Zhang, “What will 5g be?” *IEEE Journal on Selected Areas in Communications*, vol. 32, no. 6, pp. 1065–1082, June 2014.
- [2] T. S. Rappaport, S. Sun, R. Mayzus, H. Zhao, Y. Azar, K. Wang, G. N. Wong, J. K. Schulz, M. Samimi, and F. Gutierrez, “Millimeter wave mobile communications for 5g cellular: It will work!” *IEEE Access*, vol. 1, pp. 335–349, 2013.

- [3] S. Rangan, T. S. Rappaport, and E. Erkip, "Millimeter-wave cellular wireless networks: Potentials and challenges," *Proceedings of the IEEE*, vol. 102, no. 3, pp. 366–385, March 2014.
- [4] T. Bai and R. W. Heath, "Coverage and rate analysis for millimeter-wave cellular networks," *IEEE Transactions on Wireless Communications*, vol. 14, no. 2, pp. 1100–1114, Feb 2015.
- [5] J. G. Andrews, F. Baccelli, and R. K. Ganti, "A tractable approach to coverage and rate in cellular networks," *IEEE Transactions on Communications*, vol. 59, no. 11, pp. 3122–3134, November 2011.
- [6] S. Akoum, O. E. Ayach, and R. W. Heath, "Coverage and capacity in mmwave cellular systems," in *2012 Conference Record of the Forty Sixth Asilomar Conference on Signals, Systems and Computers (ASILOMAR)*, Nov 2012, pp. 688–692.
- [7] S. Singh, M. N. Kulkarni, A. Ghosh, and J. G. Andrews, "Tractable model for rate in self-backhauled millimeter wave cellular networks," *IEEE Journal on Selected Areas in Communications*, vol. 33, no. 10, pp. 2196–2211, Oct 2015.
- [8] H. S. Dhillon, R. K. Ganti, F. Baccelli, and J. G. Andrews, "Modeling and analysis of k-tier downlink heterogeneous cellular networks," *IEEE Journal on Selected Areas in Communications*, vol. 30, no. 3, pp. 550–560, April 2012.
- [9] H. S. Dhillon, R. K. Ganti, and J. G. Andrews, "A tractable framework for coverage and outage in heterogeneous cellular networks," in *2011 Information Theory and Applications Workshop*, Feb 2011, pp. 1–6.
- [10] H. S. Jo, Y. J. Sang, P. Xia, and J. G. Andrews, "Heterogeneous cellular networks with flexible cell association: A comprehensive downlink sinr analysis," *IEEE Transactions on Wireless Communications*, vol. 11, no. 10, pp. 3484–3495, October 2012.
- [11] E. Turgut and M. C. Gursoy, "Coverage in heterogeneous downlink millimeter wave cellular networks," *IEEE Transactions on Communications*, vol. PP, no. 99, pp. 1–1, 2017.
- [12] N. Deng, W. Zhou, and M. Haenggi, "Heterogeneous cellular network models with dependence," *IEEE Journal on Selected Areas in Communications*, vol. 33, no. 10, pp. 2167–2181, Oct 2015.
- [13] Z. Yazdanshenasan, H. S. Dhillon, M. Afshang, and P. H. J. Chong, "Poisson hole process: Theory and applications to wireless networks," *IEEE Transactions on Wireless Communications*, vol. 15, no. 11, pp. 7531–7546, Nov 2016.
- [14] M. A. Kishk and H. S. Dhillon, "Tight lower bounds on the contact distance distribution in poisson hole process," *IEEE Wireless Communications Letters*, vol. 6, no. 4, pp. 454–457, Aug 2017.
- [15] H. Sun, M. Wildemeersch, M. Sheng, and T. Q. S. Quek, "D2d enhanced heterogeneous cellular networks with dynamic tdd," *IEEE Transactions on Wireless Communications*, vol. 14, no. 8, pp. 4204–4218, Aug 2015.
- [16] C. h. Lee and M. Haenggi, "Interference and outage in poisson cognitive networks," *IEEE Transactions on Wireless Communications*, vol. 11, no. 4, pp. 1392–1401, April 2012.
- [17] G. Yao, N. Liu, Z. Pan, and X. You, "Coverage and rate analysis for non-uniform millimeter-wave heterogeneous cellular network," in *2016 8th International Conference on Wireless Communications Signal Processing (WCSP)*, Oct 2016, pp. 1–6.
- [18] M. Haenggi, *Stochastic Geometry for Wireless Networks*, 1st ed. New York, NY, USA: Cambridge University Press, 2012.
- [19] T. Bai, R. Vaze, and R. W. Heath, "Analysis of blockage effects on urban cellular networks," *IEEE Transactions on Wireless Communications*, vol. 13, no. 9, pp. 5070–5083, Sept 2014.
- [20] M. Ding, P. Wang, D. Lopez-Perez, G. Mao, and Z. Lin, "Performance impact of los and nlos transmissions in dense cellular networks," *IEEE Transactions on Wireless Communications*, vol. 15, no. 3, pp. 2365–2380, March 2016.
- [21] M. D. Renzo, "Stochastic geometry modeling and analysis of multi-tier millimeter wave cellular networks," *IEEE Transactions on Wireless Communications*, vol. 14, no. 9, pp. 5038–5057, Sept 2015.
- [22] X. Zhang and J. G. Andrews, "Downlink cellular network analysis with multi-slope path loss models," *IEEE Transactions on Communications*, vol. 63, no. 5, pp. 1881–1894, May 2015.